



Universiteit  
Leiden  
The Netherlands

## **Virus-host metabolic interactions: using metabolomics to probe oxidative stress, inflammation and systemic immunity**

Schoeman, J.C.

### **Citation**

Schoeman, J. C. (2016, December 20). *Virus-host metabolic interactions: using metabolomics to probe oxidative stress, inflammation and systemic immunity*. Retrieved from <https://hdl.handle.net/1887/45223>

Version: Not Applicable (or Unknown)

License: [Licence agreement concerning inclusion of doctoral thesis in the Institutional Repository of the University of Leiden](#)

Downloaded from: <https://hdl.handle.net/1887/45223>

**Note:** To cite this publication please use the final published version (if applicable).

Cover Page



Universiteit Leiden



The handle <http://hdl.handle.net/1887/45223> holds various files of this Leiden University dissertation

**Author:** Schoeman, Johannes Cornelius

**Title:** Virus-host metabolic interactions: using metabolomics to probe oxidative stress, inflammation and systemic immunity

**Issue Date:** 2016-12-20

# Chapter 5

---

## **Respiratory Syncytial virus induced oxidative stress and modulated compensatory host antioxidant responses in lung epithelial cells**

Johannes C. Schoeman, Fatiha Zaaraoui-Boutahar, Ruud Berger, Albert D. M. E. Osterhaus, Rob J. Vreeken, Arno C. Andeweg\*, and Thomas Hankemeier\*

Manuscript in preparation

\* Both authors contributed equally to the manuscript

## Abstract

The interaction between the Respiratory syncytial virus (RSV) and host antioxidant capacity has been identified as a pathogenic mechanism during infection. RSV is able to down-regulate key anti-oxidant enzymes including glutathione peroxidases, glutathione S-transferases and catalases leading to a dysregulated redox status in the host and subsequent oxidative damage. We evaluated the isoprostane profiles during an *in vitro* RSV infection of A549 cells and compared them to those of a mock-infection as a readout for oxidative stress experienced during infection. Furthermore, we used a targeted biogenic amine metabolomics platform to assess the compensatory antioxidant capacity displayed during RSV infection and complimented these measurements with targeted transcriptomics. Increased levels of isoprostanes, reflective of oxidative stress, highlights host redox biology and antioxidant capacity as determinants during the pathophysiology of an RSV infection. In addition, we found compromised sulphur metabolism during RSV infection with decreased levels of glutathione and taurine, both potent antioxidant amine metabolites. The increased glutathione pathway intermediates cysteine and cystathionine were associated with the increased expression of *LAP3*, *ANPEP* and *SQRDL* and decreased expression of *GCLC*. Increased levels of proline and spermidine allude to the upregulation of alternative host compensatory antioxidant pathways during RSV infection. This study provides further proof of the exquisite ability of RSV to modulate host redox biological responses. The work presented reveals a more concise metabolic representation of dysregulated redox status associated with RSV infection, and could aid in identifying therapeutic targets and improves risk stratification.

## Background

Respiratory syncytial virus (RSV), a member of the *Parainflaviridae* family of viruses, is the primary cause of hospitalization for lower respiratory tract infections in young children worldwide <sup>1-3</sup>. The morbidity and mortality associated with RSV infections are aggravated due to lack of an effective vaccine as well as the unpredictable nature of the infection <sup>3</sup>. In most cases, RSV is a host controlled infection exhibiting mild flu-like symptoms which resolve within 7 days, but in a small percentage of cases infection leads to life threatening bronchiolitis and/or pneumonia. Severe RSV cases are characterized by increased host immune related inflammatory lesions, that result in oxidative tissue damage, and not by RSV induced cytopathogenesis <sup>4,5</sup>.

Upon infection, RSV induces an acute oxidative pulmonary environment, compromising host antioxidant capacity and redox status leading to enhanced lung pathology, a hallmark of RSV pathogenesis <sup>6</sup>. Casola et al. identified the rapid generation and importance of reactive oxygen species (ROS) during RSV infection <sup>7</sup>, later identified as an NAD(P)H oxidase-dependent mechanism leading to increased production of superoxide ( $O_2^-$ ) during RSV infection <sup>8</sup>. Increase in superoxide coincides with increased superoxide dismutase 2 (SOD2) activity, the mitochondrial confined enzyme isomer, resulting in increased cellular hydrogen peroxide ( $H_2O_2$ ) levels <sup>9</sup>. Auto-oxidation of  $H_2O_2$  leads to increased hydroxyl radicals ( $\cdot OH$ ) modulating cellular signalling, disrupting cellular redox status, and catalysing peroxidation of macromolecules together with  $H_2O_2$ . Subsequently, Hosakote et al. identified RSV's ability to downregulate the host's antioxidant enzymes <sup>10</sup>. Using A549 cells and small airway epithelial cells as *in vitro* models, they found decreased catalase, glutathione peroxidase (GPx) and glutathione S-transferase (GST) activity after RSV infection, all antioxidant enzymes pivotal to cellular redox homeostasis <sup>9</sup>. These findings were validated *in vivo* using RSV infected BALB/c mice bronchoalveolar lavage and infant nasopharyngeal secretions, of which both reflected down-regulation of the airway antioxidant enzymes during RSV infection <sup>11</sup>. More recently Komaravelli et al. identified the deacetylation and degradation of the transcription factor NF-E2-related factor 2 (Nrf2) as an RSV mechanism able to effectively compromise and reduce the host antioxidant enzyme levels <sup>12</sup>. These findings highlight the central role of oxidative stress in RSV infection, as well as its possible role in predicting RSV disease severity. Elevated levels of ROS and increased oxidative damage have an intricate relationship with immune activation, chemotaxis of immune cells as well as inflammation <sup>13</sup>. Therefore, antioxidants have been investigated as therapeutic agents during RSV infection <sup>6</sup>. Antioxidants including butylated hydroxyanisole and melatonin were able to ameliorate RSV-induced ROS production *in vitro* <sup>14</sup> and *in vivo* <sup>15,16</sup>, significantly reducing oxidative damage and inflammation, although they were unable to effectively prevent the ability of RSV to compromise the host antioxidant capacity.

While our understanding of the RSV-host interaction has improved, our inability to identify biomarkers of RSV disease severity hampers risk stratification and clinical decision making for optimal therapeutic intervention. Thus the identification and validation of biomarkers of disease severity is of utmost importance, to address this global problem <sup>17,18</sup>. Currently the most reliable biomarker for severity is the RSV genomic load measured in nasopharyngeal aspirates which correlates strongly with disease severity <sup>19,20</sup>. Due to the increase in inflammatory lesions during severe RSV infection, Tabarani et al. reported that the cytokine signature of IL-1 $\beta$ , IL1-RA, IL-7, epidermal growth factor (EGF) and hepatocyte growth factor (HGF) could differentiate between

severe and mild disease <sup>21</sup>. Omics technologies including genome wide association studies, proteomics and metabolomics offer opportunities to study diseases, establish biomarkers for severity of the disease and prediction of prognosis, and identify targets to develop therapeutic agents. Metabolomics technologies provide a powerful tool to discover and identify intricate metabolic pathway alterations during viral infection. Whereas high throughput and quantitative metabolomics is necessary for clinical implementation using biomarker/bio-signature for clinical decision support. Studying the metabolic virus-host interaction could reveal specific metabolic alterations related to viral hijacking as well as cellular antiviral responses. Furthermore, understanding the biology of these altered metabolic pathways could lead to improved clinical decision making, and the development of broader spectrum antiviral compounds.

Here we seek to provide novel insights into the perturbed redox biology during an A549 *in vitro* RSV infection time course study. Through the use of metabolomics and targeted transcriptomics, we aim to explore the metabolic host-RSV relationship relating to redox biology, cellular antioxidant capacity and oxidative stress. The increased levels of isoprostanes provided a downstream readout for the induced oxidative stress experienced during RSV infection, while we identified dysregulation of the sulphur amine metabolism extending further than just impaired levels of glutathione during RSV infection.

## Methods

### *Chemicals and reagents*

Ultra-performance liquid chromatography (UPLC)-grade acetonitrile, isopropanol, methanol, ethyl-acetate, and water were purchased from Biosolve (the Netherlands). Glacial acetic acid was obtained from Sigma-Aldrich (St. Louis, MO). Deuterated and non-deuterated oxylipin standards were purchased either from Cayman Chemicals (Ann Arbor, MI), Biomol (Plymouth Meeting, PA), or Larodan (Malmö, Sweden).

### *Cells and viruses*

A549 cells were cultured in complete RPMI-1640 medium (Gibco Invitrogen, Carlsbad, CA, USA) supplemented with 5% (v/v) heat-inactivated fetal bovine serum (FBS; Greiner, Frickenhausen, Germany), penicillin (100 U/ml; BioWhittaker), streptomycin (100 µg/ml; BioWhittaker), L-glutamine (2 mM; BioWhittaker) at 37°C and 5% CO<sub>2</sub>. Molecularly cloned RSV-A2 (a kind donation from A.G.P. Oomens, <sup>22</sup>) was propagated on Vero118 cells at low multiplicity of infection (m.o.i.) and low passage number to avoid generation of defective interfering particles as described by van den Hoogen et al. <sup>23</sup>. Infectivity of the virus stock was measured by serial 10-fold dilutions and the titre was calculated using the method of Reed and Muench <sup>24</sup>. A549 cells were seeded in a 24-well plates at a density of  $3 \times 10^6$  cells per plate and were allowed to adhere overnight.

### *RSV infection of A549 cells and sample collection*

Overnight cultures of A549 cells were infected with RSV at a m.o.i. of 3 in serum-free medium and incubated at 37°C for 2 hours. At t=0 hours the virus inoculum or serum-free medium (mock-infection) was

removed and replaced by fresh culture media containing 5% fetal bovine serum (FBS). The infection level was determined to be between 70 to 80 % after 48 h by FACS analysis.

Cell-free culture supernatant, and cell extracts were collected at T = 0, 24, 48 and 72 hours post mock- and RSV infection. Concurrently viable cell counts per well were taken for normalisation procedures. Each sample was plated in quadruplicate, and 500  $\mu$ L culture supernatant from each replicate was collected and pooled to make a total sample volume of 2 mL. 0.8 mg butylated hydroxytoluene (BHT)/EDTA was added immediately before storage at  $-80^{\circ}\text{C}$ .

After supernatant collection, the adherent A549 cells were immediately washed twice with ice cold saline solution (0.7 % NaCl) and extracted using 200  $\mu$ L 80% ice cold methanol. As each sample was plated in quadruplicate, wells were scraped and 200  $\mu$ L of 80 % methanol from each replicate was collected and pooled to make a total sample volume of 0.8 mL; subsequently 0.8 mg butylated hydroxytoluene (BHT)/EDTA was immediately added before storage at  $-80^{\circ}\text{C}$ .

### ***Transcriptomic analyses***

Trizol homogenates from an independent A549 RSV infection experiment<sup>25</sup> were processed according to the manufacturer's instructions (Invitrogen life technologies, Carlsbad, CA, USA). Total RNA was isolated and purified using the RNeasy Mini kit (Qiagen, Hilden, Germany): 250  $\mu$ L of ethanol was added to the upper aqueous phase of the processed Trizol samples and directly transferred to the RNeasy spin columns for purification. RNA concentrations and OD 260/280 nm ratios were measured with the NanoDrop® ND-1000 UV-VIS spectrophotometer (NanoDrop Technologies, Wilmington, USA). Assessment of total RNA quality and purity was performed with the RNA 6000 Nano assay on the Agilent 2100 bioanalyzer (Agilent Technologies, Palo Alto, CA, USA). cDNA was synthesized from 2  $\mu$ g total RNA using the One-Cycle Target Labelling kit (Affymetrix, Santa Clara, CA, USA). Biotin-labelled cRNA synthesis, purification and fragmentation were performed according to standard protocols. Fragmented biotinylated cRNA was subsequently hybridised onto Affymetrix Human Genome U133 Plus 2.0 microarray chips, which were scanned with the Affymetrix GeneChip Scanner 7G. A full analysis of these experiments will be described in a later publication.

### ***Liquid Chromatography – Mass spectrometric based metabolomics***

#### ***Biogenic amine profiling***

The amine platform covers amino acids and biogenic amines employing an Accq-tag derivatization strategy adapted from the protocol supplied by Waters<sup>26</sup>. Thirty  $\mu$ L of each cell extract sample was spiked with an internal standard solution, thiol amines were reduced and released from proteins using TCEP. Proteins were then precipitated by the addition of methanol. The supernatant was transferred to a new eppendorf tube and speed-vacced to dryness. The residue was reconstituted in borate buffer (pH 8.5) and derivatized with AQC reagent. After reaction, the vials were transferred to an autosampler tray and cooled to  $10^{\circ}\text{C}$  until the injection. 1.0  $\mu$ L of the reaction mixture was injected into the UPLC-MS/MS system. An ACQUITY UPLC system with

autosampler (Waters, Etten-Leur, The Netherlands) was coupled online with a Xevo tandem quadrupole mass spectrometer (Waters) operated using QuanLynx data acquisition software (version 4.1; Waters). The samples were analyzed by UPLC-MS/MS using an Accq-Tag Ultra column (Waters). The Xevo TQ was used in the positive-ion electrospray mode and all analytes were monitored in Multiple Reaction Monitoring (MRM) using nominal mass resolution of the derivatized amino acid to the accq-tag fragment of 171 m/z.

### *Oxidative stress profiling*

The oxidative stress platform covers the isoprostanes their prostaglandin isomers and nitro-fatty acids (Schoeman et al.). Four hundred  $\mu\text{L}$  cell extract and 700  $\mu\text{L}$  medium of each sample were independently spiked with 20  $\mu\text{L}$  internal standard solution followed by acidification with 350  $\mu\text{L}$  of a pH 4.5, 0.2 M citric acid & 0.1 M disodium hydrogen phosphate buffer. Liquid-liquid extraction was used to extract the metabolites by adding 1000  $\mu\text{L}$  of butanol:ethyl acetate (1:1, v:v). After vortexing, and centrifugation (13000 rpm, 10 min at 4°C), 900  $\mu\text{L}$  of the organic phase was collected and transferred to a new tube. This extraction was repeated for a second time, and the combined organic phase were evaporated to dryness *in vacuo*. Samples were reconstituted in 30  $\mu\text{L}$  of 70 % Methanol, centrifuged (13000 rpm, 10 min at 4°C) and transferred to an insert in an LC-Vial.

The autosampler tray was kept at 5°C, and 10  $\mu\text{L}$  of sample was injected using a stacked injection into the Shimadzu LCMS 8050 system (Shimadzu, Japan) operating LabSolution software (version 4.1; Shimadzu). The metabolites were separated using a ternary gradient on a Kromasil EternityXT (1.8  $\mu\text{m}$ , 50  $\times$  2.1) column with mobile phase A (H<sub>2</sub>O with 5 mM ammonium acetate and 0.0625 % ammonium hydroxide), B (methanol with 0.2 % ammonium hydroxide) and C (2-propanol with 0.2 % ammonium hydroxide). (AkzoNobel, Amsterdam, the Netherlands). The MS was used in the negative-ion electrospray mode and all metabolites were monitored in Multiple Reaction Monitoring (MRM) using nominal mass resolution (Supplemental Table S5.1).

### *Quality control samples*

Quality control (QC) samples were used during the metabolomics analyses for quality assurance purposes. Equal volumes of each study sample were pooled to obtain the QC pool. A set of QC samples were then included during the analyses of the experimental groups, and evenly distributed through the randomized samples prior to LC-MS analyses. In addition, independent duplicate samples (10 - 15 %) were randomly selected where sample volume allowed for it. Using the QC samples and duplicate samples, a double-quality-control approach was applied and only metabolites for which both duplicate and QC samples showed an RSD < 30% were considered for biological interpretation.

### *Data processing, normalisation and statistical analyses*

For the biogenic amine platform, peak integration was performed with TargetLynx - MassLynx (v4.1). For the oxidative stress platform metabolites, peak integration was done using the Shimadzu software Labsolutions (v 5.72). For both platforms, the peak areas of targets were corrected using their respective internal standards.

To correct for the variance in cell counts across the RSV and mock-infection time course study, metabolite normalisation was done to ensure accurate comparisons. We used the total intracellular amine metabolites to

correct for the variance in cell counts across the different time points, due to their tight regulation in cellular metabolism. To prevent skewing of the normalisation procedure, we only used the total amine sum of the “stable” middle two quantiles (50 % quartile; normalised area ratios ranked from high to low) to normalise our groups. In vitro normalisation based on cell counts is a well-established procedure, and was used as a reference during our normalisation approach. Pearson correlation between cell counts and the middle 50 % total amines gave a high degree of correlation with  $R^2 = 0.813$  which supported and served as validation of our approach (supplementary Figure S5.1).

Data pre-treatment consisted of zero replacement in the case of missing data, followed by data normalization, log transformation and auto scaling using MetaboAnalyst 3.0<sup>27</sup>. Using MetaboAnalyst 3.0, multivariate statistical analyses were done on both groups and all time points and included principal component analyses (PCA) and partial least squares-discriminant analyses (PLS-DA). Univariate approaches were done between groups at 24h and 48h post infection independently and included Mann-Whitney U test, fold change, and false discovery rate. Metabolites identified as significant were used for pathway analyses using MetaboAnalyst v3.0. GraphPad Prism 6 (GraphPad, La Jolla, CA, USA) was used in Spearman correlation analyses and rendering of graphs.

For transcriptomics, data were log<sub>2</sub>-transformed and normalized by variance stabilising normalisation (VSN)<sup>28</sup>. Statistically significant differential expression for each probe set was assessed using the Linear Model for MicroArray data (limma)<sup>29</sup> expressed as the fold change in expression between infected and uninfected conditions (False discovery rate cut-off of 0.05). Probe sets with the highest differential expression were chosen as represented for the gene product.

## Results

An *in vitro* time course (t = 0, 24, 48, and 72 hours) study of RSV- and mock (empty vector) - infected A549 cells was used to metabolically investigate the pathogenic mechanisms associated with redox biology during RSV infection. A synchronised RSV infection in A549 cells was achieved with approximately a 75 % infection level measured at 48h post infection. Within 24h post infection the first cytopathic effects were noted, these subtle morphological changes were followed by cell detachment at 48h and ultimately cell death resulted in decreased cell numbers at 72h. Culture medium and cell lysate were collected sequentially and subjected to metabolomics analyses.

### ***RSV infection-induces oxidative stress during infection***

To assess oxidative stress, we used a dedicated oxidative stress metabolomics method, profiling a wide range of isoprostanes (ROS peroxidised lipids) while ensuring resolution from the cyclooxygenase derived prostaglandins (structural isomers of the isoprostanes). By comparing intra- and extracellular isoprostane profiles of the RSV infected cells compared with control cells, a readout can be provided for oxidative stress experienced during infection<sup>30,31</sup>. Significantly increased levels of isoprostanes (fold change (FC)>2 compared to control) were present already at 24h and even more so at 48h post RSV infection, indicative of oxidative stress (Figure 5.1). Only two intracellular isoprostanes were detected compared to seven identified in the

extracellular medium. High levels of especially 8-iso-PGE<sub>2</sub> and 8-iso-15-keto-PGF<sub>2α</sub>, the downstream metabolite of 8-iso-PGF<sub>2α</sub>, were present within the extracellular medium. A strong positive correlation ( $p < 0.05$ ) was observed in the RSV group by individual Spearman correlation analyses between the intra- and extracellular levels (Figure S5.2) of each of the two detected isoprostanes (8-iso-PGE<sub>2</sub> and 5-iPF<sub>2α</sub>-VI). The higher presence of isoprostanes in the extracellular environment is not surprising as these peroxidised lipids are known to be actively excreted from the cells. In addition, detection of a wide range of isoprostanes confirmed the presence of oxidative stress more strongly, compared to single metabolite analyses.

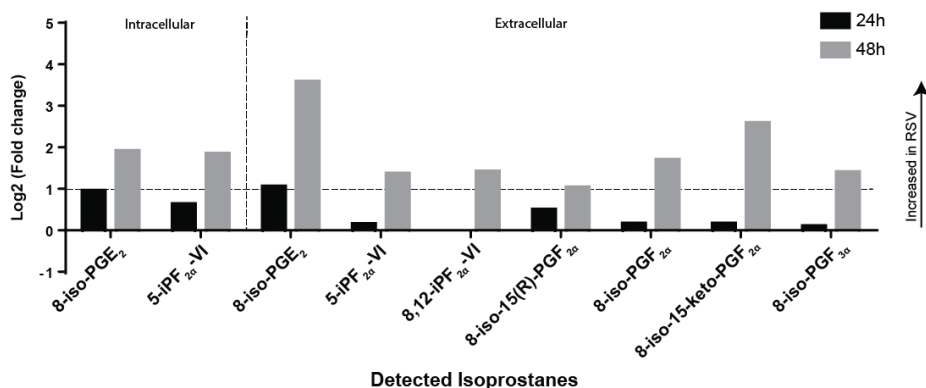


**Figure 5.1: Oxidative stress profiling of RSV infected A549 cells.** Fold changes (FCs) compared to control are plotted for the RSV groups compared to corresponding mock time points, indicating high levels of lipid peroxidation metabolites present during RSV infection. The horizontal dashed line indicates a FC = 2.

### *Metabolic evaluation of host antioxidant capacity*

Host defence mechanisms against oxidative stress include the host antioxidant capacity responsible for scavenging and neutralising free radicals. Therefore, we studied the effect of RSV infection and induced oxidative stress on the biogenic amine metabolic pathways, which are at the core of the host compensatory metabolic antioxidant system. Targeted metabolomics profiling was used to characterize the intracellular amine profiles of RSV-infected and mock-infected A549 cells at different time points post infection  $t = 0, 24, 48,$  and  $72$  hours. A total of 74 amine metabolites were profiled, with 39 complying with the predefined criteria of our QC procedures (Table S5.2). Using an explorative PCA analysis (Figure 5.2), 66 % of the variation in the data was explained in the first two principal components and indicated partial natural RSV and mock differentiation 24h post infection, and more clearly 48h post infection. No clear separation was found within the mock group during the time course. Using the supervised PLS-DA model (Figure S5.3) improved clustering and differentiation between Mock and RSV was observed at both the 24h and 48h post infection time points. The model had strong predictive value, with  $Q^2 = 0.64$  and  $R^2 = 0.85$  when using a leave-one-out-cross-validation

method. Permutation testing using 100 permutations indicated good model fit with  $p < 0.01$ . Twelve metabolites were identified as significant with variables important in projection (VIP) scores  $> 1$  (Table S5.3) of which five: cysteine, taurine, glutathione, cystathionine and  $\gamma$ -glutamylglutamine belong to the sulphur amine metabolism. In both PCA and PLS-DA the 72h RSV infected cells showed comparatively large intra-group variation, suggesting that for certain samples within the 72h time point the RSV infection definitely affected the cellular integrity reducing the reliability of the generated biological data, hence we will primarily focus on the 24h and 48h time points. Alterations at the 24h time point reflect early RSV induced metabolic perturbations compared to the 48h time points which possibly provides a resulting readout from these initial alterations.

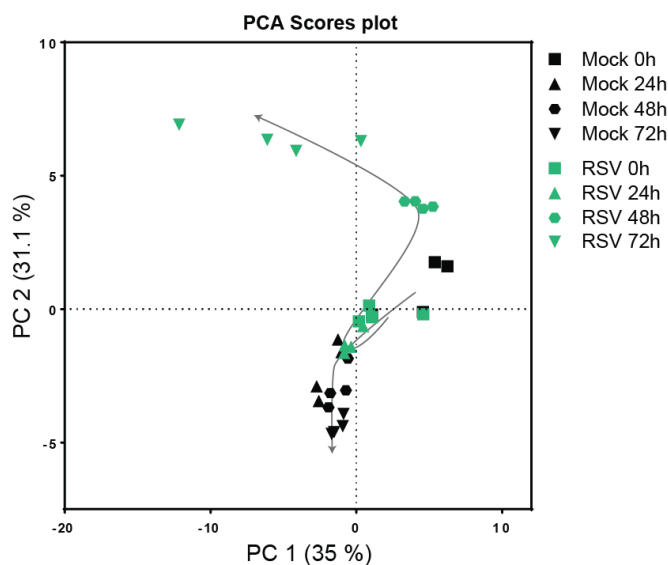


**Figure 5.2:** Principal component analyses of the RSV and mock-infected cells' intracellular amine profiles. The PCA shows clustering and no differentiation between RSV and mock-infection at  $t = 0h$  groups. Only after 24h do the RSV infection time points differentiate from those of the mock-infection.

For a more in depth look into the amine response during RSV infection, we used strict univariate statistical approaches including Mann-Whitney  $U$ -test ( $p < 0.05$ ) and fold-change analyses with  $FC > 2$  (increased in RSV) or  $FC < 0.5$  (decreased in RSV), on the 24h and 48h time points to identify early and later responding perturbations. At 24h post infection, only one metabolite  $\gamma$ -glutamylglutamine adhered to the strict univariate conditions with significantly increased levels in the RSV infected cells (Table 5.1, Figure S5.4). Although, we did also identify reduced levels of glutathione, together with increased levels of glutamic acid, aspartate and gamma-aminobutyric acid (GABA) as early responding metabolites (Table 5.1). At 48h post infection, 20 metabolites were significantly altered of which 16 were increased within the RSV group relative to

the control group (Table 5.1, Figure S5.5). Q-values based on the false discovery rate are reported for each metabolite identified as significant.

**Table 5.1:** Significant amine metabolites altered at 24h and 48h post RSV infection.

Metabolite	Mann-Witney U-test (p < 0.05)	Fold Change <sup>#</sup>		False discovery rate (q-value)
		(FC > 2)	(FC < 0.5)	
<b>24h post RSV infection</b>				
Glutamic acid*	9.42E-6	1.59	-	3.67E-4
Aspartate*	3.32E-4	1.33	-	0.006
Gamma-aminobutyric acid*	0.001	1.33	-	0.012
Glutathione*/**	0.0013	-	0.67	0.012
γ-glutamyl-glutamine**	0.006	2.53	-	0.051
<b>48h post RSV infection</b>				
Sarcosine**	6.50E-08	-	0.26	1.59E-06
Glutathione**	8.13E-08	-	0.04	1.59E-06
Cystathionine**	2.49E-07	3.04	-	3.23E-06
Gamma-aminobutyric acid	7.06E-07	-	0.41	6.89E-06
Cysteine**	1.36E-06	32.17	-	1.06E-05
Lysine	5.33E-06	3.07	-	3.46E-05
2-Amino adipic acid**	1.03E-05	13.84	-	5.72E-05
Proline**	1.73E-05	9.77	-	8.18E-05
Taurine**	1.89E-05	-	0.43	8.18E-05
Valine	9.54E-05	2.17	-	3.06E-04
Arginine	0.0001	2.56	-	3.06E-04
Methionine sulfoxide	0.0001	2.05	-	3.92E-04
Serine	0.0002	2.56	-	5.17E-04
Spermidine**	0.0002	6.13	-	5.21E-04
Ethanolamine**	0.0007	2.71	-	0.001
Ornithine	0.0007	2.96	-	0.001
o-Acetylserine**	0.0007	32.45	-	0.001
Beta-alanine	0.003	2.66	-	0.004
Homoarginine	0.005	2.22	-	0.007
NG-Hydroxyarginine	0.03	3.75	-	0.04

# FC > 2 indicates increased levels in the RSV group, whereas FC < 0.5 indicates reduced levels in the RSV group.

\* Significant early (t=24h) responding metabolites (p<0.05 & q<0.05) not adhering to the strict FC cut-off criterion.

\*\* Indicates amine metabolites identified with PLS-DA VIP scores > 1

Subsequently, we used these 20 significantly altered metabolites to do a metabolic pathway analysis, in order to identify the pathways most affected during RSV infection and to direct our transcriptomics analyses (Figure S5.6). Pathway analysis reveals the most prominent amine metabolic pathways, irrespective of up- and down regulation, using the Kegg metabolic pathway database, through assigning a p-value based on the number of hits per pathway (Table S5.4). Interestingly, inspection of the top five amine pathways affected during RSV infection identified three pathways related to sulphur metabolism and the innate cellular antioxidant capacity. These three pathways included: i. cysteine and methionine metabolism, ii. glutathione metabolism, and iii. sulphur metabolism, supporting our findings of increased oxidative stress during RSV infection. The other two

pathways identified were the arginine and proline pathways as well as the non-specific aminoacyl-tRNA biosynthesis process - the latter will not be discussed further here. Through using the KEGG database, we extracted the gene IDs of the enzymes functioning within these metabolic pathways for a targeted transcriptomics approach.

### ***Targeted transcriptomics of amine metabolism***

To complement the metabolomics data, we screened 204 amine metabolic related genes for differential expression (Table 5.2) in an independent A549 RSV infection experiment which included genes related to the sulphur containing amines, arginine, proline, glutamate and glycine metabolic pathways. Messenger RNA transcripts were measured at 6h, 12h and 24h post RSV infection. Eleven gene transcripts were significantly differentially expressed 24h post infection when compared with mock-infected control cells with  $\log_2(\text{FC}) > 1$  (increased -  $\text{FC} > 2$ ) and  $\log_2(\text{FC}) < -1$  (decreased -  $\text{FC} < 0.5$ ). Early responding genes, 6h post RSV infection, were found in glutamate metabolism with upregulation of *ASS1* and *GFPT2*. The arginine-proline metabolism indicated significant upregulation during RSV infection with increased *LAP3*, *SAT1*, *SMOX*, and *P4HA2* levels. Although metabolomics identified cysteine, glutathione and sulphur metabolism as significantly affected during RSV infection, transcriptomics identified only subtle changes within the first 24h. Only *SQRDL* expression was significantly increased in sulphur metabolism, together with noticeable changes in *SDSL* (increased) and *GCLC* (decreased) levels in cysteine metabolism. The glutathione metabolism showed significant increased expression of *LAP3* and *ANPEP* gene targets, whereas Glutathione-S-transferase indicated differential regulation of isomers with noticeable upregulation of *GSTK1* and *GSTO1* and downregulation of *GSTA4*.

Individually, both omics approaches are able to provide insights into the altered amine metabolism experienced during RSV infection, but integration of the data could prove even more insightful. Hence, next we assessed the integrated metabolic pathways covering the metabolites and transcripts identified as significant.

Table 5.2: Amine directed transcriptomic gene target list and response during RSV infection

Amine metabolic pathway (KEGG pathway ID)	Gene ID targets	Gene targets identified significantly increased during RSV infection (log <sub>2</sub> (FC))			Gene targets identified significantly decreased during RSV infection (log <sub>2</sub> (FC))		
		6h	12h	24h	6h	12h	24h
Arginine and Proline metabolism, n=50 (hsa00330)	GATM, GAMT, CKM, CKMT1A, CKMT2, CKR, CKMT1B, AZIN2, AGMAT, ODC1, SRM, SMS, AMD1, AOCI, SMOX, ALDH2, ALDH3A2, ALDH1B1, ALDH7A1, ALDH9A1, CNND1P, CNND1P2, CARN1, SAT2, SAT1, MAOB, MAOA, NOS1, NOS2, NOS3, ARG2, ARG1, OAT, PYCRL, PYCR2, PYCRL, PRODH, ALDH4A1, ALDH18A1, LAP3, P4HA2, P4HA3, P4HA1, PRODH2, GOT1, GOT2, HOGA1, DAO, L3H1PDIH	-	LAP3 (1.29)	LAP3 (2.87) P4HA2 (1.02) SAT1 (1.23) SMOX (1.38) ALDH2* (0.79) CKP* (0.88)	-	-	-
Thauric and hypotaurine metabolism, n=11 (hsa00430)	CDO1, GAD1, GAD2, CSAD, GADL1, ADO, GGT7, GGT6, GGT1, GGT5, BAAT	-	-	-	-	-	-
Sulphur metabolism, n=10 (hsa00920)	PAPSS2, PAPSS1, BPNT1, IMPAD1, SUOX, CYCS, ETH1EL, MPST, TST, SQRD1	-	SQRD1* (0.88)	SQRD1 (1.935)	-	-	-
Cysteine and methionine, n=38 (hsa00270)	CTH, CBS, CBSL, BMTF, BMT2, MTR, MAT2B, MAT3A, MAT2A, MTAP, MRU1, APIP, ENOPH1, ADL1, TAT, IL4H, DSNMT1, DSNMT3A, DSNMT3B, AHCYL2, AHCYL1, AHCY, BCAT2, BCAT1, AGXT2, GCLC, GCLM, GSS, MPST, LDHAL6A, LDHAL6B, LDHA, LDHB, LDHG, MDH1, MDH2, SDS, SDSL	-	-	SDSL* (0.85)	-	-	GCLC** (-0.72)
Glycine, serine and threonine metabolism, n=27 (hsa00260)	SHMT2, SHMT1, PSPH, PSAT1, PHGDH, GLYCTK, PGAM1, PGAM2, PGAM4, BPGM, GRHPR, GCAT, ALAS1, ALAS2, AOC3, AOC2, GLDC, AMT, DLD, GCSI, AGXT, CHDH, DMGDH, PPOX, SARPH, GNMT, SRR	BPGM* (0.73)	-	ALAS1* (0.86)	-	-	PSPH (-1.04)
Gluathione metabolism, n=41 (hsa00480)	GGGT, OPLAH, ANPEP, GSTA5, GSTA2, GSTA4, GSTO2, GSTM4, GSTE3, GSTH1, GSTM3, MGST1, MGSTE3, GSTP1, GSTM1, GSTM5, MGST2, GSTA1, GSTM2, GSTA3, GSTO1, GSTT2B, GSTK1, GSR, HPGDS, IDH1, IDH2, PGD, G6PD, TXNDC12, GPX6, GPX7, GPX2, GPX3, GPX1, GPX5, GPX8, GPX4, RRM1, RRM2B, RRM2	-	ANPEP* (0.76) LAP3 (1.29)	ANPEP* (0.86) GSTK1* (0.73) GSTO1* (0.72) LAP3 (2.87)	-	-	GSTA4** (-0.92)
Alanine, aspartate and glutamate metabolism, n=27 (hsa00250)	DDO, ASN5M, NIT2, GTP2, GTP, ASS1, ASL, ADSSL1, ADSS, ADSL, NAT8L, RIMK1B, RIMK1A, FOLH1, ASPA, ABAT, ALDH5A1, GLUD2, GLUD1, GLUL, CAD, GLS2, GLS, CFS1, GHP2, GHP2, GHP1, PPA1	ASS1 (1.03) GHP2* (0.90)	ASS1* (0.93) GHP2* (0.78)	ABAT (1.00)	-	-	ADSSL1 (-1.03) GLS** (-0.71)

Genes with an absolute fold change log<sub>2</sub>(FC) value of > 1 were identified as upregulated and genes with an absolute log<sub>2</sub>(FC) < -1 were identified as downregulated respectively (and a false discovery rate of 0.05).

\* noticeable upregulation with log<sub>2</sub>(FC) in between 0.7 - 0.99; \*\* noticeable downregulation with log<sub>2</sub>(FC) in between -0.7 - -0.99

## ***Integrated amine pathway investigation***

### *Cysteine, glutathione and sulphur metabolism*

The metabolic multivariate and univariate results revealed an altered redox homeostatic environment within the A549 cells post RSV infection. The interdependent and interlinked nature of i. cysteine and methionine metabolism, ii. glutathione metabolism and iii. sulphur metabolism enables us to reconstruct an elementary metabolic picture to visualize the induced metabolic changes upon RSV infection (Figure 5.3). Although only subtle transcriptomic changes are found in these metabolic pathways, integrating the transcriptomics results illuminate and support the metabolic observations. Increased levels of cysteine and cystathionine strongly oppose the reduced glutathione levels resulting from RSV infection. Serine, possibly supplemented via pyruvate (glycolysis) due to upregulation of serine hydratase like (*SDSL*), fuelled cysteine biosynthesis (Figure 5.3A). Transcriptomics revealed two perturbations able to explain the compromised glutathione levels (Figure 5.3B). Down-regulation of gamma-glutamylcysteine synthetase (*GCLC*) blocked cysteine and glutamate joining (ligation), the first step of glutathione synthesis. Secondly, significant upregulation of both cytosol aminopeptidase (*LAP3*) and aminopeptidase N (*ANPEP*) resulted in an increased gamma-glutamyl cycle catalysing the hydrolyses of glutathione and supplementing intracellular cysteine levels. Since our sample prep method makes use of a reducing step, we report the total glutathione levels and are unable to discriminate between the reduced and oxidised glutathione species. Although this can be seen as a drawback, by reporting the total glutathione pool size we do provide a glimpse in the synthesis of this metabolite during RSV infection, which reveals significant impairment. Furthermore, metabolomics revealed significant decreased levels of taurine derived from cysteine suggesting RSV-induced mechanisms were at play. The upregulated transcript *SQRDL* encodes for sulfide:quinone oxidoreductase catalysing the first step in hydrogen sulphide ( $H_2S$ ) to thiosulphate<sup>32</sup> (Figure 5.3C). Increased  $H_2S$  is the direct consequence of increased cysteine and is a recently discovered labile biological signalling gasotransmitter<sup>33</sup>. It should be mentioned that for all the metabolites shown in Figure 5.3, the mock-infection indicated stable levels across the time course indicating cellular homeostasis. Collectively, metabolomics and transcriptomics reflect an altered redox homeostasis through dysregulated cysteine and glutathione metabolism during RSV infection, supported by the observations of increased levels of isoprostanes indicative of oxidative stress.

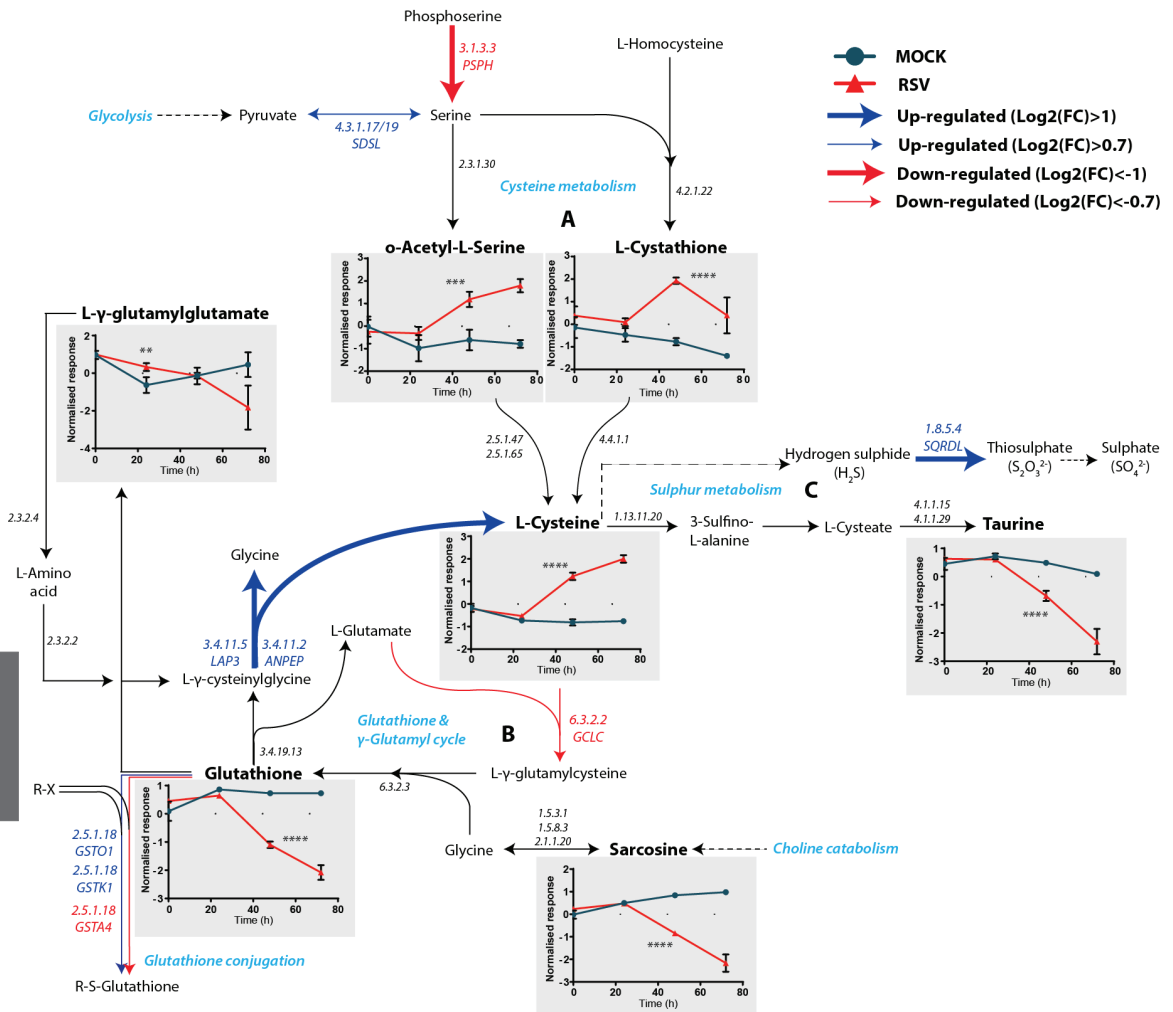


**Figure 5.3: Integrative cysteine (A), glutathione (B) and sulphur (C) metabolism during RSV infection.** Increased cysteine and cystathionine metabolites allude to upregulation of the cysteine biosynthesis via glycolysis supplementing serine levels during RSV infection. Significantly decreased levels of glutathione result from the blockage of L-gamma-glutamylcysteine synthesis due to downregulation of *GCLC* expression, but also due to increased breakdown via *LAP3* and *ANPEP* supplementing intracellular cysteine levels. Metabolomics identified significant decreased levels of taurine, and transcriptomics revealed increased expression *SQRDL* functioning in the sulphur metabolism. Collectively the cysteine and glutathione metabolism reflects an altered redox homeostasis during RSV infection. Differentially expressed gene transcripts represent only the first 24h post infection. The metabolic pathway is reconstructed using the Kegg Homo sapiens pathway with enzymes EC number(s) displayed for reactions, and significant metabolites indicated with \*\*  $p < 0.01$ . \*\*\*  $p < 0.001$  and \*\*\*\*  $p < 0.0001$ . *ANPEP* – aminopeptidase N; *GCLC* – gamma-glutamylcysteine synthetase; *GSTA4* – glutathione-S-transferase alpha 4; *GSTK1* – glutathione-S-transferase kappa 1; *GSTO1* – glutathione-S-transferase omega 1; *LAP3* – cytosol aminopeptidase; *PSPH*; phosphoserine phosphatase; *SDSL* – serine hydratase like; *SQRDL* - sulfide:quinone oxidoreductase.

*Arginine and proline metabolism*

Increased intracellular levels of proline, arginine, ornithine, spermidine and decreased levels of gamma-aminobutyric acid (GABA) defined the RSV infection's induced metabolic alterations of the arginine and proline metabolic pathways (Figure 5.4). All the metabolites shown, except for GABA, indicated stable levels during the mock-infection time course. Data integration alludes to an important role for glutamate during RSV infection (Figure 5.4A). Glutamate can flux through GABA to supplement the tricarboxylic acid (TCA) cycle, but can also supplement glutamine levels. Increased expression of glutamine-fructose-6-phosphate transaminase 2 (*GFPT2*) and 1 (*GFPT1*) transcripts suggests a glutamate-glutamine flux into the amino-sugar metabolism (Figure 5.4B). This finding is further supported with the reduced expression of glutaminase (*GLS*) reducing the back conversion of glutamine to glutamate. Secondly, aspartate utilisation was directed towards arginine biosynthesis, feeding into the ornithine-putrescine pathway (Figure 5.4C). Putrescine was subsequently used as precursor for spermidine biosynthesis, but also acted as a precursor for the biosynthesis of GABA via upregulated secondary pathways (Figure 5.4D). GABA derived from aspartate was most likely used to fuel the TCA cycle via succinate, supported by the increased expression of GABA transferase (*ABAT*) and decreased levels of intracellular GABA during RSV infection. Although several pathways can explain the significantly increased levels of proline, upregulation of cytosol aminopeptidase (*LAP3*) suggests increased proline specific peptide catabolism resulting in increased levels of proline (Figure 5.4E).

Collectively, the presented results reveal increased oxidative stress during RSV infection together with significant alteration in the host amine metabolism, compromising its compensatory anti-oxidant capacity.

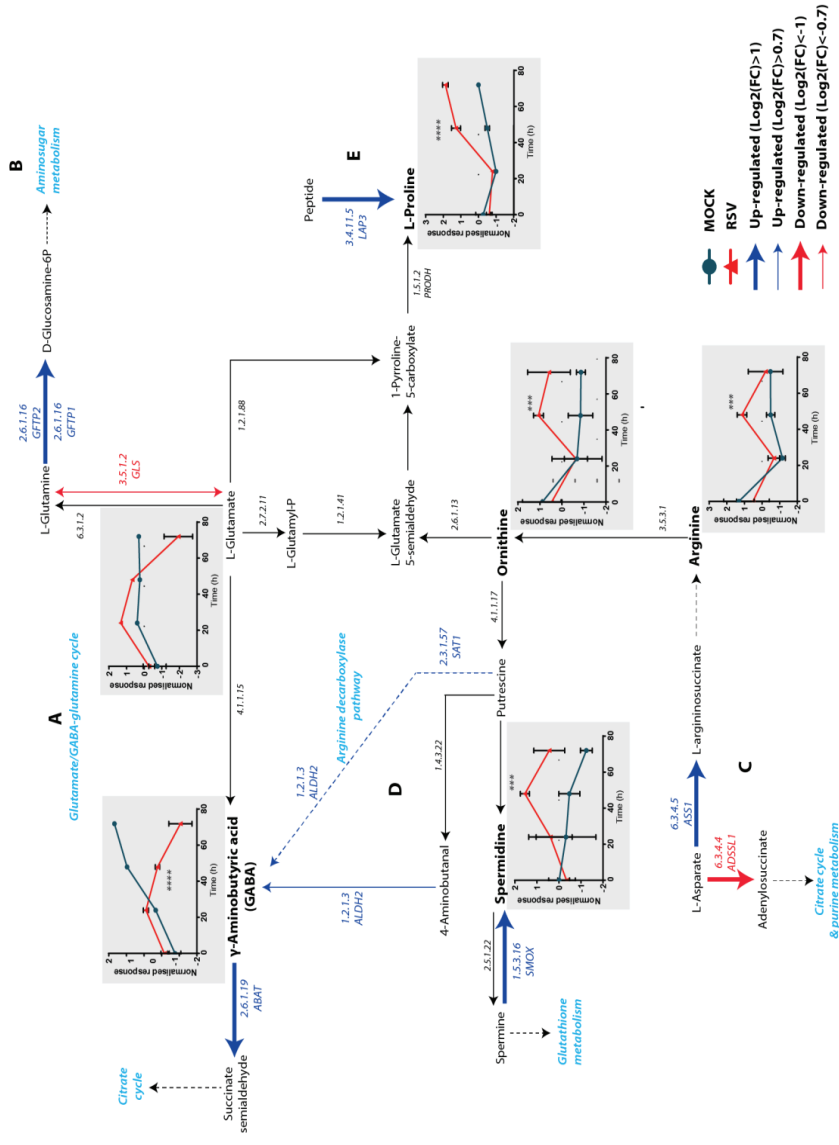


**Figure 5.4: Integrative arginine and proline metabolic pathway during RSV infection.** During RSV infection glutamate (A) is fluxed via glutamine into the amino-sugar metabolism (B). Aspartate (C) fuelled the arginine, ornithine pathway to synthesise putrescine which acted as precursor for GABA (D) synthesis via secondary pathways to fuel the TCA cycle. Increased intracellular levels of proline in the RSV infected cells possibly resulted from increased peptide hydrolysis (E). Simultaneously, upregulation of spermidine, the polyamine precursor was also found in the RSV cells. Differentially expressed gene transcripts represent only the first 24h post infection. The metabolic pathway is reconstructed using the Kegg Homo sapiens pathway with enzymes EC number(s) displayed for reactions, and significant metabolites indicated with \*\*\*  $p < 0.001$  and \*\*\*\*  $p < 0.0001$ . *ABAT* - *GABA transferase*; *ADSSLL1* - *adenylosuccinate synthase*; *ALDH2* - *aldehyde dehydrogenase*; *ASST1*; *argininosuccinate synthase*; *GFTP1/2* - *glutamine-fructose-6-phosphate transaminase 1/2*; *L-AP3* - *cytosol aminopeptidase*; *S-AT* - *sulfate adenylyltransferase*; *SMOX* - *spermine oxidase*.

## Discussion

Here we used a targeted and comprehensive oxidative stress profiling method to report on the presence of isoprostanes as a readout of oxidative stress induced during RSV infection of A549 cells. Next, we evaluated the host's metabolic compensatory mechanisms through targeting the host's amine metabolism and its role during RSV infection. The integration of targeted amine metabolic transcriptomics data supported the observed metabolic perturbations, while additionally providing context and alluding to metabolic fate and flux. Oxidative stress has been identified as a core pathogenic route during RSV infection. RSV exploits the increased ROS through modulating cellular signalling, while also resulting in oxidative tissue injury observed during *in vitro* and *in vivo* RSV infections<sup>8,10–12,34</sup>. Several *in vitro* and *in vivo* studies have identified a compromised cellular antioxidant system based on reduced levels of GPx, GST and catalase diminishing the cell's glutathione reserves and inhibiting cellular redox control mechanisms during RSV infection<sup>10–12,14–16</sup>.

Evaluating oxidative stress is a complex process, with the direct measurement of ROS through the use of electrodes being a cumbersome approach and mostly confined to *in vitro* studies. Therefore, the measurement of downstream products like the isoprostanes, which reflects the presence and/or increase in ROS, is a more attractive approach *in vitro* as well as *in vivo*. The increased intra- and extracellular isoprostanes reveal increased ROS and high levels of oxidative stress experienced during RSV infection. Significantly, increased levels of the isoprostanes: 8-iso-PGE<sub>2</sub> and 5-iPF<sub>2 $\alpha$</sub> -VI were detected intracellularly, while extracellularly these two metabolites, together with the well characterized 8-iso-PGF<sub>2 $\alpha$</sub>  among others were also detected. We identified 8-iso-PGE<sub>2</sub> as the most abundant intra- and extracellular isoprostane and suggest this could be a more sensitive oxidative stress marker than the F-series isoprostanes. The mechanisms showing how increased lipid peroxidation within the cell affects membrane integrity, enhances inflammatory signalling while also interacting with the cellular apoptotic pathways have been reviewed extensively in<sup>35–37</sup>.

Next, studying the host's compensatory capacity revealed glutathione, taurine, and the sulphur metabolism are significantly compromised during RSV infection, corroborating the findings of increased isoprostanes. Our results show that RSV infection has the ability to reduce the total intracellular glutathione pool size through down-regulating gamma-glutamylcysteine synthetase, while up-regulating glutathione recycling ( $\gamma$ -glutamyl cycle) via the action of peptidases, adding to cysteine levels. The increased cystathionine and cysteine could also result from the host's upregulation, via serine, in an attempt to restore the compromised antioxidant state and curb the oxidative stress experienced during RSV infection. The reported metabolic results here support the current available literature relating to RSV infection's ability to modulate the cellular glutathione capacity. Interestingly, although we detected increased isoprostanes 24h post infection, the biogenic amine metabolism revealed initial resilience since no significant changes were found 24h post RSV infection (Figure 5.3). Although after 48h its clear that RSV has completely overwhelmed the cellular glutathione and sulphur metabolism, impairing the host compensatory mechanisms.

Cysteine is an important intermediate metabolite in sulphur metabolic pathways, producing hydrogen sulphide (H<sub>2</sub>S), via transsulphuration reactions, an important physiological gasotransmitter. Sulfide:quinone oxidoreductase (*SQRDL*) is a highly efficient mitochondrial enzyme capable of rapidly oxidation H<sub>2</sub>S to the

downstream metabolite thiosulfate<sup>32</sup>. Recently Li et al. reported on the broad inhibitory effect of H<sub>2</sub>S on RSV syncytium formation and virus assembly/release. They also found that during RSV infection, airway epithelial cells had a reduced ability to generate and maintain intracellular H<sub>2</sub>S levels<sup>38</sup>. Another link to sulphur metabolism is the work by Komaravelli et al. where they reveal the engineering capacity of RSV to inhibit the activation of the transcription factor NF- E2-related factor 2 (Nrf2)<sup>39</sup>. Nrf2 regulates the gene expression of the cellular antioxidant enzymes through binding to the gene promoter regions. Interestingly, H<sub>2</sub>S has the ability to activate the Nrf2 transcription pathway, inducing the expression of the antioxidant genes<sup>40</sup>. Thus the early up-regulation of *SQRDL* (<12h) provides more insight into RSV's capacity to orchestrate the failure of the host innate antioxidant pathways, ensuring RSV survival.

Taurine is an abundant biogenic amine, and is normally found in high concentrations in tissues exposed to elevated levels of oxidants where it elicits protective anti-inflammatory signalling and ROS inhibition abilities<sup>41–45</sup>. Hence, taurine presents a compensatory route to inhibit ROS production via cysteine catabolism, with cysteine dioxygenase determining the flux between taurine - and glutathione synthesis. As taurine levels follow a trend similar to glutathione, our results indicate that the RSV regulation of the cellular antioxidant capacity extends further than glutathione alone. However, transcriptomics levels at 24 hours was unable to provide context for explaining the mechanism leading to reduced taurine levels. Jong et al. has identified taurine as a regulator of mitochondrial protein synthesis, ensuring electron transport chain integrity and protecting the mitochondria against excessive superoxide generation<sup>46</sup>. Taurine also scavenges hypochlorite (ClO<sup>-</sup>) produced by infiltrating leucocytes (neutrophils and monocytes via the myeloperoxidase pathway) to form the less toxic Tau-Cl<sup>47</sup>, which is actively transported into the leucocytes where it down-regulates pro-inflammatory mediators TNF- $\alpha$ , IL-6 and IL-8<sup>48–50</sup>. Severe RSV disease is characterised by increased levels of TNF- $\alpha$  and IL-6 among others<sup>21</sup>. Thus, RSV's ability to deplete cellular taurine levels further compromise host ability to rectify the antioxidant dysregulation and dampen the strong pro-inflammatory response during acute infection.

We think that significant increased levels of intracellular proline during RSV infection is an important novel finding, although we cannot fully explain it yet. In recent years, our understanding of the functions of proline in cellular physiology has improved significantly. Upregulated proline biosynthesis and its accumulation has been reported in fungal, plant and mammalian cells in response to cellular stress, especially H<sub>2</sub>O<sub>2</sub><sup>51–54</sup>. Proline functions include the scavenging of intracellular ROS, inhibition of ROS-mediated apoptosis via activation of the Akt survival pathway, and sustaining cellular energy<sup>51,53–55</sup>. A proline protection model against H<sub>2</sub>O<sub>2</sub> stress proposed by Natarajan et al. suggests that proline catabolism via *PRODH* in the mitochondria is central to its antioxidant ability. *PRODH* activity helps support oxidative phosphorylation and ATP formation and prevents decreases in NADPH/NADP<sup>+</sup>, maintaining redox homeostasis<sup>54</sup>. Increased expression of cytosol aminopeptidase capable of reducing intracellular glutathione is possibly responsible in part for increased proline. Thus, it is possible to hypothesize that the increased proline is a host adaptation as an alternative antioxidant pathway to compensate for the RSV induced dysregulated glutathione metabolism. In addition to proline, increased levels of spermidine, a polyamine mediating antioxidant and anti-inflammatory activity, were also measured in RSV infected cells<sup>56</sup>. Ha et al. identified the antioxidant function of spermidine as directly scavenging ROS, especially singlet oxygen and hydroxyl radicals<sup>57</sup>.

Lastly, the integration between metabolomics and transcriptomics alluded to the role of the multifaceted amino acid glutamate during RSV infection. Glutamate seems to flux via glutamine into the aminosugar biosynthesis pathway, which is responsible for the formation of glycosylation motifs. The post-translational glycosylations of viral proteins enhance their diversity, and play important roles during the viral life cycle as well as immune evasion<sup>58</sup>. GABA, a well characterised neurotransmitter, is also a glutamate intermediate via glutamate decarboxylase expressed in A549 cells<sup>59</sup> supplementing the TCA cycle. Metabolomics and transcriptomics revealed the upregulation of secondary pathways via aspartate and arginine to synthesize GABA to provide cellular energy. Further experimentation is needed to disentangle the role of RSV and the host in redirecting GABA synthesis, as energy production is essential for the survival of both host and virus.

Metabolomics is a powerful tool to elucidate viral-host interactions on the metabolic level, and is far more informative compared to single metabolite assays. The complementing of metabolomics with transcriptomics analyses strengthens the understanding of the metabolic relationship of RSV and the human host. Recently, the importance of sulphur metabolism during RSV infection has been identified as a key pathogenic pathway<sup>38</sup> and warrants further investigation. Therapeutic intervention targeting the cellular antioxidant capacity needs to be extended further than just the cellular glutathione reserves but should also target H<sub>2</sub>S metabolism. Identifying patients having a compromised antioxidant capacity could possibly help in predicting RSV disease severity. The role of proline as an antioxidant and inhibitor of mitochondria-dependent apoptotic pathways needs to be evaluated further to understand the beneficial or detrimental role for the host.

## Conclusion

Through the use of metabolomics and targeted transcriptomics, we explore the metabolic relationship between RSV and the host relating to redox biology, cellular antioxidant capacity and oxidative stress. The early detection of increased levels of lipid peroxidation markers reveal the capacity of RSV to induce oxidative stress in A549 cells upon infection. Furthermore, metabolomics found an impaired glutathione metabolism and compromised antioxidant capacity in A549 cells during RSV infection in accordance with literature. In addition, we found dysregulation to a much wider extent in the host's sulphur metabolism with increased cysteine and cystathionine levels and decreased levels of taurine following a similar trend as glutathione. Transcriptomics supported our metabolic findings and also alluded to the pathogenic role of sulfide:quinone oxidoreductase in further dampening anti-viral host responses in rapidly metabolising H<sub>2</sub>S derived from increased cysteine. Since the host is not a passive bystander, we also identified the upregulation of secondary antioxidant pathways resulting in increased levels of proline and spermidine. The host's biogenic amine resilience and compensatory mechanism (<24h) was unsustainable against RSV after 48 and especially 72 hours. The significant metabolic changes related to glutathione, cysteine, taurine and proline (especially their ratios) may be good disease severity markers and are worth to be clinically further investigated. Ultimately, enhancing these pathways for the host beneficial metabolic compensatory mechanisms maybe even be possible targets for drug development.

## Acknowledgements

This study was supported by the NWO-ZonMW grant number 435002027, and the Virgo consortium, funded by the Dutch government project number FES0908. We would also like to thank Shimadzu for their loan of the LCMS-8050 system and their technical support.

## References

1. Borchers, A. T., Chang, C., Gershwin, M. E. & Gershwin, L. J. Respiratory syncytial virus--a comprehensive review. *Clin. Rev. Allergy Immunol.* **45**, 331–79 (2013).
2. Collins, P. L. & Melero, J. A. Progress in understanding and controlling respiratory syncytial virus: still crazy after all these years. *Virus Res.* **162**, 80–99 (2011).
3. Hall, C. B. *et al.* The burden of respiratory syncytial virus infection in young children. *N. Engl. J. Med.* **360**, 588–98 (2009).
4. McNamara, P. S. & Smyth, R. L. The pathogenesis of respiratory syncytial virus disease in childhood. *Br. Med. Bull.* **61**, 13–28 (2002).
5. Openshaw, P. J. M. & Tregoning, J. S. Immune Responses and Disease Enhancement during Respiratory Syncytial Virus Infection. *Clin. Microbiol. Rev.* **18**, 541–555 (2005).
6. Garofalo, R. P., Kolli, D. & Casola, A. Respiratory syncytial virus infection: mechanisms of redox control and novel therapeutic opportunities. *Antioxid. Redox Signal.* **18**, 186–217 (2013).
7. Casola, A. *et al.* Oxidant tone regulates RANTES gene expression in airway epithelial cells infected with respiratory syncytial virus. Role in viral-induced interferon regulatory factor activation. *J. Biol. Chem.* **276**, 19715–22 (2001).
8. Liu, T. *et al.* Reactive oxygen species mediate virus-induced STAT activation: role of tyrosine phosphatases. *J. Biol. Chem.* **279**, 2461–9 (2004).
9. Hosakote, Y. M., Liu, T., Castro, S. M., Garofalo, R. P. & Casola, A. Respiratory syncytial virus induces oxidative stress by modulating antioxidant enzymes. *Am. J. Respir. Cell Mol. Biol.* **41**, 348–57 (2009).
10. Hosakote, Y. M., Liu, T., Castro, S. M., Garofalo, R. P. & Casola, A. Respiratory syncytial virus induces oxidative stress by modulating antioxidant enzymes. *Am. J. Respir. Cell Mol. Biol.* **41**, 348–57 (2009).
11. Hosakote, Y. M. *et al.* Viral-mediated inhibition of antioxidant enzymes contributes to the pathogenesis of severe respiratory syncytial virus bronchiolitis. *Am. J. Respir. Crit. Care Med.* **183**, 1550–60 (2011).
12. Komaravelli, N. *et al.* Respiratory syncytial virus infection down-regulates antioxidant enzyme expression by triggering deacetylation-proteasomal degradation of Nrf2. *Free Radic. Biol. Med.* **88**, 391–403 (2015).
13. Harijith, A., Ebenezer, D. L. & Natarajan, V. Reactive oxygen species at the crossroads of inflammasome and inflammation. *Front. Physiol.* **5**, 352 (2014).
14. Hosakote, Y. M. *et al.* Antioxidant mimetics modulate oxidative stress and cellular signaling in airway epithelial cells infected with respiratory syncytial virus. *Am. J. Physiol. Lung Cell. Mol. Physiol.* **303**, L991–1000 (2012).
15. Castro, S. M. *et al.* Antioxidant treatment ameliorates respiratory syncytial virus-induced disease and lung inflammation. *Am. J. Respir. Crit. Care Med.* **174**, 1361–9 (2006).
16. Huang, S.-H., Cao, X.-J., Liu, W., Shi, X.-Y. & Wei, W. Inhibitory effect of melatonin on lung oxidative stress induced by respiratory syncytial virus infection in mice. *J. Pineal Res.* **48**, 109–16 (2010).
17. Shah, S. S., Ambroggio, L. & Florin, T. A. Biomarkers for Predicting Illness Severity in Children With Acute Lower Respiratory Tract Infections. *J. Pediatric Infect. Dis. Soc.* **4**, 189–91 (2015).
18. Brown, P. M., Schneeberger, D. L. & Piedimonte, G. Biomarkers of respiratory syncytial virus (RSV) infection: specific neutrophil and cytokine levels provide increased accuracy in predicting disease severity. *Paediatr. Respir. Rev.* **16**, 232–40 (2015).

19. Hasegawa, K. *et al.* Respiratory syncytial virus genomic load and disease severity among children hospitalized with bronchiolitis: Multicenter cohort studies in the United States and Finland. *J. Infect. Dis.* **211**, 1550–1559 (2015).
20. El Saleeby, C. M., Bush, A. J., Harrison, L. M., Aitken, J. A. & Devincenzo, J. P. Respiratory syncytial virus load, viral dynamics, and disease severity in previously healthy naturally infected children. *J. Infect. Dis.* **204**, 996–1002 (2011).
21. Tabarani, C. M. *et al.* Novel inflammatory markers, clinical risk factors and virus type associated with severe respiratory syncytial virus infection. *Pediatr. Infect. Dis. J.* **32**, e437–42 (2013).
22. Oomens, A. G. P., Megaw, A. G. & Wertz, G. W. Infectivity of a human respiratory syncytial virus lacking the SH, G, and F proteins is efficiently mediated by the vesicular stomatitis virus G protein. *J. Virol.* **77**, 3785–98 (2003).
23. van den Hoogen, B. G. *et al.* Excessive production and extreme editing of human metapneumovirus defective interfering RNA is associated with type I IFN induction. *J. Gen. Virol.* **95**, 1625–33 (2014).
24. Reed, L.J. and Muench, H. A simple method of estimating fifty percent endpoints. *Am. J. Hyg.* **27**, 493–7 (1938).
25. van Diepen, A. *et al.* Quantitative proteome profiling of respiratory virus-infected lung epithelial cells. *J. Proteomics* **73**, 1680–1693 (2010).
26. Noga, M. J. *et al.* Metabolomics of cerebrospinal fluid reveals changes in the central nervous system metabolism in a rat model of multiple sclerosis. *Metabolomics* **8**, 253–263 (2012).
27. Xia, J., Mandal, R., Sinelnikov, I. V., Broadhurst, D. & Wishart, D. S. MetaboAnalyst 2.0—a comprehensive server for metabolomic data analysis. *Nucleic Acids Res.* **40**, W127–33 (2012).
28. Pradervand, S. *et al.* Impact of normalization on miRNA microarray expression profiling. *RNA* **15**, 493–501 (2009).
29. Smyth, G. K. Linear models and empirical bayes methods for assessing differential expression in microarray experiments. *Stat. Appl. Genet. Mol. Biol.* **3**, Article3 (2004).
30. Montuschi, P., Barnes, P. J. & Roberts, L. J. Isoprostanes: markers and mediators of oxidative stress. *FASEB J.* **18**, 1791–800 (2004).
31. Morrow, J. D. & Roberts, L. J. The isoprostanes: unique bioactive products of lipid peroxidation. *Prog. Lipid Res.* **36**, 1–21 (1997).
32. Jackson, M. R., Melideo, S. L. & Jorns, M. S. Human sulfide:quinone oxidoreductase catalyzes the first step in hydrogen sulfide metabolism and produces a sulfane sulfur metabolite. *Biochemistry* **51**, 6804–15 (2012).
33. Carter, R. N. & Morton, N. M. Cysteine and hydrogen sulphide in the regulation of metabolism: Insights from genetics and pharmacology. *J. Pathol.* **238**, 321–332 (2016).
34. Jamaluddin, M., Tian, B., Boldogh, I., Garofalo, R. P. & Brasier, A. R. Respiratory syncytial virus infection induces a reactive oxygen species-MSK1-phospho-Ser-276 RelA pathway required for cytokine expression. *J. Virol.* **83**, 10605–15 (2009).
35. Chandra, J., Samali, A. & Orrenius, S. Triggering and modulation of apoptosis by oxidative stress. *Free Radic. Biol. Med.* **29**, 323–33 (2000).
36. Martindale, J. L. & Holbrook, N. J. Cellular response to oxidative stress: signaling for suicide and survival. *J. Cell. Physiol.* **192**, 1–15 (2002).
37. Sinha, K., Das, J., Pal, P. B. & Sil, P. C. Oxidative stress: the mitochondria-dependent and mitochondria-independent pathways of apoptosis. *Arch. Toxicol.* **87**, 1157–80 (2013).
38. Li, H. *et al.* Role of hydrogen sulfide in paramyxovirus infections. *J. Virol.* **89**, 5557–68 (2015).
39. Komaravelli, N. *et al.* Respiratory syncytial virus infection down-regulates antioxidant enzyme expression by triggering deacetylation-proteasomal degradation of Nrf2. *Free Radic. Biol. Med.* **88**, 391–403 (2015).
40. Hourihan, J. M., Kenna, J. G. & Hayes, J. D. The gasotransmitter hydrogen sulfide induces nrf2-target genes by inactivating the keap1 ubiquitin ligase substrate adaptor through formation of a disulfide bond between cys-226 and cys-613. *Antioxid. Redox Signal.* **19**, 465–81 (2013).
41. Schuller-Levis, G. B. & Park, E. Taurine: new implications for an old amino acid. *FEMS Microbiol. Lett.* **226**, 195–202 (2003).

42. Gordon, R. E., Shaked, A. A. & Solano, D. F. Taurine protects hamster bronchioles from acute NO<sub>2</sub>-induced alterations. A histologic, ultrastructural, and freeze-fracture study. *Am. J. Pathol.* **125**, 585–600 (1986).
43. Gurujeyalakshmi, G., Wang, Y. & Giri, S. N. Suppression of bleomycin-induced nitric oxide production in mice by taurine and niacin. *Nitric Oxide* **4**, 399–411 (2000).
44. Giri, S. N., Blaisdell, R., Rucker, R. B., Wang, Q. & Hyde, D. M. Amelioration of bleomycin-induced lung fibrosis in hamsters by dietary supplementation with taurine and niacin: biochemical mechanisms. *Environ. Health Perspect.* **102 Suppl**, 137–47 (1994).
45. Schaffer, S. W., Azuma, J. & Mozaffari, M. Role of antioxidant activity of taurine in diabetes. *Can. J. Physiol. Pharmacol.* **87**, 91–9 (2009).
46. Jong, C. J., Azuma, J. & Schaffer, S. Mechanism underlying the antioxidant activity of taurine: prevention of mitochondrial oxidant production. *Amino Acids* **42**, 2223–32 (2012).
47. Weiss, S. J., Klein, R., Slivka, A. & Wei, M. Chlorination of taurine by human neutrophils. Evidence for hypochlorous acid generation. *J. Clin. Invest.* **70**, 598–607 (1982).
48. Park, E., Alberti, J., Quinn, M. R. & Schuller-Levis, G. Taurine chloramine inhibits the production of superoxide anion, IL-6 and IL-8 in activated human polymorphonuclear leukocytes. *Adv. Exp. Med. Biol.* **442**, 177–82 (1998).
49. Park, E., Jia, J., Quinn, M. R. & Schuller-Levis, G. Taurine chloramine inhibits lymphocyte proliferation and decreases cytokine production in activated human leukocytes. *Clin. Immunol.* **102**, 179–84 (2002).
50. Park, E., Quinn, M. R., Wright, C. E. & Schuller-Levis, G. Taurine chloramine inhibits the synthesis of nitric oxide and the release of tumor necrosis factor in activated RAW 264.7 cells. *J. Leukoc. Biol.* **54**, 119–24 (1993).
51. Krishnan, N., Dickman, M. B. & Becker, D. F. Proline modulates the intracellular redox environment and protects mammalian cells against oxidative stress. *Free Radic. Biol. Med.* **44**, 671–81 (2008).
52. Kaul, S., Sharma, S. S. & Mehta, I. K. Free radical scavenging potential of L-proline: Evidence from in vitro assays. *Amino Acids* **34**, 315–320 (2008).
53. Hare, P. D. & Cress, W. A. Metabolic implications of stress-induced proline accumulation in plants. *Plant Growth Regul.* **21**, 79–102 (1997).
54. Natarajan, S. K. *et al.* Proline dehydrogenase is essential for proline protection against hydrogen peroxide-induced cell death. *Free Radic. Biol. Med.* **53**, 1181–91 (2012).
55. Chen, C. & Dickman, M. B. Proline suppresses apoptosis in the fungal pathogen *Colletotrichum trifolii*. *Proc. Natl. Acad. Sci. U. S. A.* **102**, 3459–64 (2005).
56. Jamwal, S. & Kumar, P. Spermidine ameliorates 3-nitropropionic acid (3-NP)-induced striatal toxicity: Possible role of oxidative stress, neuroinflammation, and neurotransmitters. *Physiol. Behav.* **155**, 180–7 (2016).
57. Ha, H. C. *et al.* The natural polyamine spermine functions directly as a free radical scavenger. *Proc. Natl. Acad. Sci. U. S. A.* **95**, 11140–5 (1998).
58. Vigerust, D. J. & Shepherd, V. L. Virus glycosylation: role in virulence and immune interactions. *Trends Microbiol.* **15**, 211–8 (2007).
59. Xiang, Y.-Y. *et al.* A GABAergic system in airway epithelium is essential for mucus overproduction in asthma. *Nat. Med.* **13**, 862–7 (2007).

## Supplementary Information

## Supplementary Tables

Table S5.1 Oxidative stress profiling target list for LC-MS/MS method.

Compound class	Compound name	Precursor ion> Product ion (m/z)	CE (V)	Dwell time (msec)	MS Polarity	Internal standard	Lipid Maps ID
<b>Identified metabolites based on standards</b>							
Isoprostane	2,3-dinor-11B-iso-PGF <sub>2</sub> a	325.00>145.20	20	20	Neg	(d4) PGF <sub>2</sub> a	LMFA03010011
Isoprostane	2,3-dinor-8-iso-PGF <sub>2</sub> a	325.10>237.20	12	20	Neg	(d4) 8-iso-PGF <sub>2</sub> a	LMFA03110010
Isoprostane	5- $\alpha$ IP <sub>2</sub> a VI	353.30>115.05	22	40	Neg	(d11) 5- $\alpha$ IP <sub>2</sub> a VI	LMFA03110010
Isoprostane	8,12-IP <sub>2</sub> a VI	353.30>115.05	22	40	Neg	(d11) 8,12-IP <sub>2</sub> a VI	
Isoprostane	8-iso-13,14-dihydro-PGF <sub>2</sub> a	353.30>183.10	25	20	Neg	(d4) 8-iso-PGF <sub>2</sub> a	LMFA03110009
Isoprostane	8-iso-15-keto-PGF <sub>2</sub>	349.10>287.20	16	20	Neg	(d4) 8-iso-PGF <sub>2</sub>	LMFA03110005
Isoprostane	8-iso-15-keto-PGF <sub>2</sub> a	351.10>315.15	22	20	Neg	(d4) 8-iso-PGF <sub>2</sub> a	
Isoprostane	8-iso-15-keto-PGF <sub>2</sub> b	351.10>315.15	22	20	Neg	(d4) 8-iso-PGF <sub>2</sub> a	
Isoprostane	8-iso-15-R-PGF <sub>2</sub> a	353.30>193.20	25	20	Neg	(d4) 8-iso-PGF <sub>2</sub> a	
Isoprostane	8-iso-PGA1	335.10>273.15	19	20	Neg	(d4) PGA2	LMFA03110008
Isoprostane	8-iso-PGA2	333.10>271.20	15	20	Neg	(d4) PGA2	
Isoprostane	8-iso-PGE1	353.30>317.20	15	20	Neg	(d4) PGE1	LMFA03110002
Isoprostane	8-iso-PGE2	351.10>271.15	17	20	Neg	(d4) 8-iso-PGE2	LMFA03110003
Isoprostane	8-iso-PGF1a	355.30>311.10	22	20	Neg	(d9) 8-iso-PGF1a	
Isoprostane	8-iso-PGF2a (15- $\beta$ 2 $\alpha$ -IsoP)	353.30>193.20	25	20	Neg	(d4) 8-iso-PGF <sub>2</sub> a	LMFA03110001
Isoprostane	8-iso-PGF3a	351.10>307.15	19	20	Neg	(d4) 8-iso-PGF <sub>2</sub> a	LMFA03110007
Isoprostane	IP <sub>1</sub> a-IV	353.30>127.10	22	20	Neg	(d4) IP <sub>1</sub> a-VI	
Prostaglandins	13,14-dihydro-PGF <sub>2</sub> a	353.30>183.10	25	20	Neg	(d4) PGF <sub>2</sub> a	LMFA03010079
Prostaglandins	PGA1	335.10>273.15	19	20	Neg	(d4) PGA2	LMFA03010005
Prostaglandins	PGA2	333.10>271.20	15	20	Neg	(d4) PGA2	LMFA03010005
Prostaglandins	PGD2	351.10>271.15	17	20	Neg	(d4) PGD2	LMFA030100035
Prostaglandins	PGD3	349.10>269.20	17	20	Neg	(d4) PGD2	LMFA03010004
Prostaglandins	PGE1	353.30>317.20	15	20	Neg	(d4) PGE1	LMFA03010134
Prostaglandins	PGE2	351.10>271.15	17	20	Neg	(d9) PGE2	LMFA030100003
Prostaglandins	PGE3	349.10>269.20	17	20	Neg	(d9) PGE2	LMFA03010135
Prostaglandins	PGF1a	355.30>311.10	22	20	Neg	(d9) 8-iso-PGF1a	LMFA03010137
Prostaglandins	PGF2a	353.30>193.20	25	20	Neg	(d4) PGF <sub>2</sub> a	LMFA03010002
Prostaglandins	PGF3a	351.10>307.15	19	20	Neg	(d4) PGF <sub>2</sub> a	LMFA03010138
<b>Internal standards</b>							
Isoprostane	5- $\alpha$ IP <sub>2</sub> a-VI-d11	364.20>115.05	22	20	Neg	<i>na</i>	LMFA03110011
Isoprostane	8-iso-PGF2-d4	355.30>275.25	18	20	Neg	<i>na</i>	LMFA03010008
Isoprostane	8-iso-PGF1a-d9	364.20>320.25	23	20	Neg	<i>na</i>	
Isoprostane	8-iso-PGF2a-d4	357.30>197.15	20	20	Neg	<i>na</i>	
Isoprostane	IP <sub>2</sub> a-VI-d4	357.20>114.90	22	20	Neg	<i>na</i>	
Isoprostane	8,12-iso-IP <sub>2</sub> a-VI-d11	364.20>115.05	23	40	Neg	<i>na</i>	
Prostaglandins	PGD2-d4	355.30>275.25	18	20	Neg	<i>na</i>	LMFA03010007
Prostaglandins	PGF2a-d4	357.30>197.15	20	20	Neg	<i>na</i>	LMFA03010006
Prostaglandins	PGE2-d9	359.90>280.25	18	20	Neg	<i>na</i>	
Prostaglandins	PGE1-d4	357.30>321.20	15	20	Neg	<i>na</i>	
Prostaglandins	PGA2-d4	336.90>275.00	11	20	Neg	<i>na</i>	
Reference	Cuda	339.30>214.25	24		Neg	<i>na</i>	

**Table S5.2** Overview of the detected amine metabolites. Normalised\* amine responses are presented as internal standard corrected area ratios, with the % RSD reflecting the biological variation per time point n = 4.

Metabolite	Mock Infection			RSV Infection			HMDB Identifier
	t0h Normalised Area ratio (%RSD)	t24h Normalised Area ratio (%RSD)	t72h Normalised Area ratio (%RSD)	t0h Normalised Area ratio (%RSD)	t24h Normalised Area ratio (%RSD)	t48h Normalised Area ratio (%RSD)	
Putrescine	0.007 (26.2)	0.011 (24.01)	0.012 (20.13)	0.006 (24.97)	0.016 (18.8)	0.007 (7.03)	0.006 (17.22)
Ethanolamine	0.21 (22.04)	0.22 (67.85)	0.24 (14.23)	0.11 (74.88)	0.26 (21.38)	0.26 (21.38)	0.26 (14.42)
Ornithine	0.056 (70.52)	0.028 (68.44)	0.032 (14.65)	0.029 (24.48)	0.021 (34.25)	0.028 (10.1)	0.033 (28.22)
Lysine	0.12 (52.98)	0.03 (22.15)	0.05 (16.09)	0.05 (57.13)	0.03 (15.12)	0.04 (4.42)	0.04 (32.19)
Glycine	0.34 (25.07)	0.31 (15.45)	0.27 (17.83)	0.26 (15.45)	0.32 (9.02)	0.26 (4.58)	0.15 (14.82)
Sarcosine	0.24 (4.86)	0.46 (5.71)	0.98 (3.22)	0.22 (7.16)	0.36 (14.55)	0.06 (4.61)	0.03 (4.49)
Beta-alanine	0.024 (104.53)	0.014 (56.53)	0.019 (34.09)	0.008 (52.97)	0.015 (17.68)	0.017 (26.14)	0.015 (9.73)
Alanine	0.069 (30.85)	0.069 (16.25)	0.422 (1.22)	0.054 (24.62)	0.055 (17.26)	0.051 (15.36)	0.048 (16.15)
Gamma-amino butyric acid	0.018 (4.49)	0.04 (4.35)	0.119 (5.44)	0.114 (5.44)	0.043 (15.08)	0.016 (3.75)	0.012 (8.66)
Serine	0.79 (47.41)	0.44 (27.49)	0.24 (4.77)	0.42 (34.4)	0.36 (20.07)	0.24 (16.82)	0.24 (16.82)
Cystathionine	0.025 (4.34)	0.028 (9.33)	0.03 (5.36)	0.027 (11)	0.027 (10.47)	0.03 (6.06)	0.025 (5.55)
Proline	4 (63.4)	1.7 (13.54)	3.9 (13.26)	1.7 (21.07)	1.8 (12.91)	12.9 (34.01)	44 (42.06)
Valine	0.09 (38.02)	0.05 (16)	0.05 (5.16)	0.05 (34.06)	0.05 (34.06)	0.04 (12.54)	0.03 (20.67)
Threonine	0.44 (35.64)	0.32 (9.67)	0.42 (4.44)	0.26 (35.06)	0.26 (12.11)	0.21 (4.38)	0.16 (18.6)
Cysteine	0.051 (42.57)	0.024 (12.42)	0.025 (20.38)	0.034 (24.86)	0.026 (12.86)	0.274 (31.43)	1.73 (63.15)
Taurine	2.3 (4.43)	3.6 (10.58)	3.3 (3.15)	2 (4.99)	2.6 (15.12)	0.5 (8.98)	0.2 (14.41)
Isoleucine	0.29 (37.03)	0.18 (11.89)	0.33 (5.75)	0.16 (38.05)	0.15 (14.09)	0.12 (3.79)	0.08 (20.52)
Leucine	0.054 (36.31)	0.033 (9.59)	0.053 (5.18)	0.029 (39.73)	0.028 (10.06)	0.023 (6.21)	0.016 (21.21)
4-Hydroxyproline	0.34 (29.82)	0.349 (13.57)	1.141 (3.15)	0.359 (9.78)	0.28 (16.03)	0.188 (12.24)	0.124 (15.82)
Asparagine	0.4 (33.42)	0.39 (10.14)	1.07 (3.2)	0.64 (1.01)	0.29 (14.39)	0.24 (5.08)	0.15 (20.86)
Glycylglycine	0.4 (34.67)	0.389 (9.87)	1.065 (4.7)	0.644 (1.96)	0.234 (37.06)	0.236 (4.56)	0.146 (17.31)
Aspartic acid	0.22 (12.94)	0.42 (3.63)	0.51 (9.32)	0.46 (7.26)	0.44 (9.66)	0.15 (7.22)	0.08 (24.95)
O-Phosphoethanolamine	0.003 (7.21)	0.004 (8.3)	0.007 (8.13)	0.002 (45.44)	0.004 (20.51)	0.002 (48.47)	0.002 (25.86)
Glutamine	1 (42.91)	0.7 (11.82)	1.3 (3.86)	1 (2.92)	0.5 (13.26)	0.3 (6.24)	0.2 (24.37)
Glutamic acid	1.3 (12.78)	2.9 (8.77)	4 (4.97)	3.3 (4.41)	1.2 (7.62)	1.4 (1.76)	0.6 (15)
o-Acetylserrine	0.033 (82.81)	0.006 (61.43)	0.01 (39.87)	0.016 (103.65)	0.014 (51.15)	0.176 (64.92)	0.939 (50.16)
Methionine	0.65 (49.09)	0.43 (14.37)	0.45 (6.97)	0.39 (65.3)	0.35 (18.84)	0.23 (11.9)	0.17 (19.11)
Histidine	0.003 (22.03)	0.002 (19.96)	0.004 (16.75)	0.003 (16.75)	0.002 (15.28)	0.001 (11.57)	0.001 (48.27)
Spermidine	0.003 (54.41)	0.004 (87.2)	0.003 (42.32)	0.002 (23.14)	0.002 (42.82)	0.006 (18.28)	0.004 (46.7)
2-Aminoadipic acid	0.037 (99.03)	0.017 (29.35)	0.015 (10.72)	0.011 (47.92)	0.015 (18.11)	0.067 (28.29)	0.347 (36.29)
Methionine sulfoxide	0.022 (45.24)	0.012 (8.65)	0.015 (8.59)	0.011 (36.49)	0.011 (10.94)	0.01 (14.13)	0.008 (10.66)
Phenylalanine	0.11 (34.46)	0.07 (8.81)	0.08 (9.6)	0.06 (27.78)	0.06 (22.63)	0.05 (13.06)	0.04 (19.49)
Arginine	0.96 (49.1)	0.26 (11.74)	0.56 (8.11)	0.48 (73.89)	0.27 (14.33)	0.4 (17.33)	0.3 (34.54)
Citrulline	0.006 (40.59)	0.007 (67.03)	0.008 (52.84)	0.005 (38.92)	0.005 (47.65)	0.005 (32.1)	0.005 (28.15)
Tyrosine	1.3 (28.33)	1 (9.43)	1.9 (7.75)	0.8 (28.05)	0.8 (10.15)	0.6 (5.45)	0.4 (15.59)
Homoarginine	0.0004 (31.94)	0.0007 (35.37)	0.0006 (10.34)	0.0005 (28.64)	0.0007 (13.68)	0.0005 (34.01)	0.0003 (36.55)
NG-Hydroxyarginine	0.007 (64.72)	0.003 (85.3)	0.007 (91.16)	0.003 (40.61)	0.01 (99.62)	0.009 (44.62)	0.006 (72.27)
γ-Glutamylglutamine	0.003 (22.99)	0.001 (34.67)	0.002 (14.92)	0.003 (13.91)	0.002 (14.12)	0.001 (57.35)	0 (79.33)
Glutathione	0.049 (41.92)	0.236 (12.98)	0.148 (8.37)	0.066 (5.7)	0.126 (18.51)	0.003 (17.59)	0.001 (21.7)

HMDB – Human metabolome database

\* Amino internal standard corrected area ratios were normalised using the amine sum of the 2 middle quartiles refer to Methods - Data processing, normalisation and statistical analyses

**Table S5.3:** Metabolites Identified with PLS-DA component 1 VIP scores > 1

Rank	Metabolite	VIP score
1	Cysteine	1.7812
2	Taurine	1.7167
3	Glutathione	1.6985
4	o-Acetylserine	1.6821
5	Proline	1.6798
6	2-Aminoadipic acid	1.6176
7	Sarcosine	1.5935
8	Glutamine	1.5912
9	Cystathionine	1.3605
10	Ethanolamine	1.2058
11	Spermidine	1.0772
12	gamma-Glutamylglutamine	1.0229

**Table S5.4:** Pathway analyses of the 20 significant metabolites identified at 48h post infection.

Metabolic pathway	Total	Hits	Raw p	-Log (p)	Holm adjust	FDR	Impact
Aminoacyl-tRNA biosynthesis	75	6	1.47E-05	11.126	0.0011778	0.0006869	0.11268
Arginine and proline metabolism	77	6	1.72E-05	10.972	0.0013565	0.0006869	0.40852
Cysteine and methionine metabolism	56	5	5.16E-05	9.8718	0.0040256	0.0013763	0.28083
Glutathione metabolism	38	4	0.0001729	8.6627	0.013314	0.0034583	0.27351
Sulfur metabolism	18	3	0.000316	8.0598	0.024016	0.0050559	0.07205
Glycine, serine and threonine metabolism	48	4	0.0004335	7.7437	0.032508	0.0057793	0.18577
Pantothenate and CoA biosynthesis	27	3	0.0010828	6.8282	0.080129	0.012067	0.07286
beta-Alanine metabolism	28	3	0.0012067	6.7199	0.08809	0.012067	0.32319
D-Arginine and D-ornithine metabolism	8	2	0.0016074	6.4332	0.11573	0.014288	0
Taurine and hypotaurine metabolism	20	2	0.010308	4.5748	0.73187	0.082464	0.33094
Lysine biosynthesis	32	2	0.025436	3.6716	1	0.18499	0.16762
Propanoate metabolism	35	2	0.030088	3.5036	1	0.20059	0.085
Nitrogen metabolism	39	2	0.036777	3.3029	1	0.22632	0
Lysine degradation	47	2	0.051686	2.9626	1	0.29535	0.16238
Biotin metabolism	11	1	0.08365	2.4811	1	0.44613	0
Cyanoamino acid metabolism	16	1	0.11944	2.1249	1	0.5972	0
Selenoamino acid metabolism	22	1	0.16064	1.8286	1	0.7222	0.00482
Thiamine metabolism	24	1	0.17396	1.7489	1	0.7222	0
Alanine, aspartate and glutamate metabolism	24	1	0.17396	1.7489	1	0.7222	0.10256
Sphingolipid metabolism	25	1	0.18055	1.7117	1	0.7222	0
Valine, leucine and isoleucine biosynthesis	27	1	0.19357	1.6421	1	0.73742	0.01325
Methane metabolism	34	1	0.23763	1.437	1	0.8641	0.01751
Glycerophospholipid metabolism	39	1	0.26769	1.3179	1	0.87541	0.05562
Valine, leucine and isoleucine degradation	40	1	0.27356	1.2962	1	0.87541	0
Butanoate metabolism	40	1	0.27356	1.2962	1	0.87541	0.01067
Primary bile acid biosynthesis	47	1	0.31346	1.1601	1	0.9645	0.00822
Pyrimidine metabolism	60	1	0.38211	0.96204	1	1	0
Porphyrin and chlorophyll metabolism	104	1	0.56934	0.56328	1	1	0.00167

**Total** - total number of compounds in the Kegg Pathway

**Hits** - actually matched number from the uploaded data

**Raw p** - the original p value calculated from the enrichment analysis

**Holm adjust** - p value adjusted by Holm-Bonferroni method

**FDR** - p-value adjusted using False Discovery Rate

**Impact** - pathway impact value calculated from pathway topology analysis.

## Supplementary figures

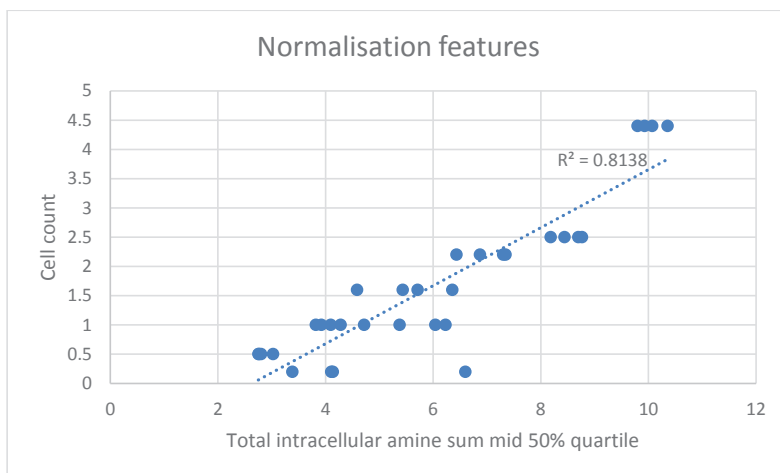


**Figure S5.1:** Correlation between cell counts and total intracellular amines (middle 50 % quartile) profiles. As amine metabolism is tightly regulated they give a more accurate reflection of the intracellular environment. Choosing the mid 50 amine quartile represents the most stable amines, and its total sum could be used as a normalization feature across the different time points. Plotting the total amine sums with the respective cell counts reflected a high degree of correlation, and acted as proof of concept.

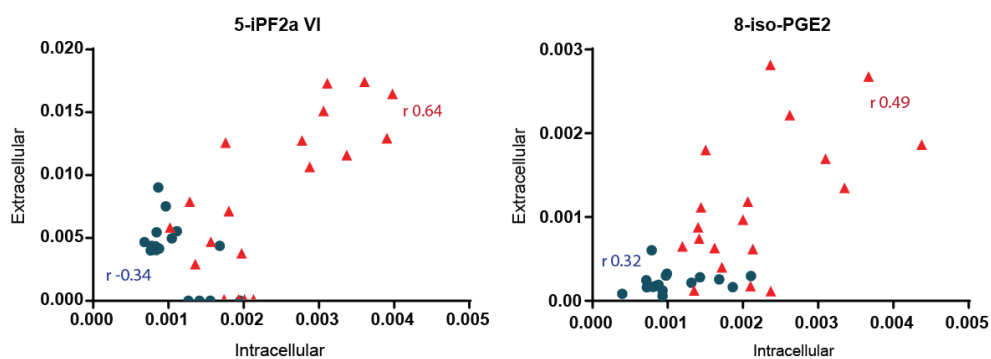


**Figure S5.2:** Spearman correlation analyses of intra- and extracellular detected isoprostanes. Spearman correlation analyses between the two isoprostanes detected both intra- and extracellular in the RSV (orange - triangle) and Mock (blue - circle) samples. The Spearman coefficient  $r$  is indicated on the graph.

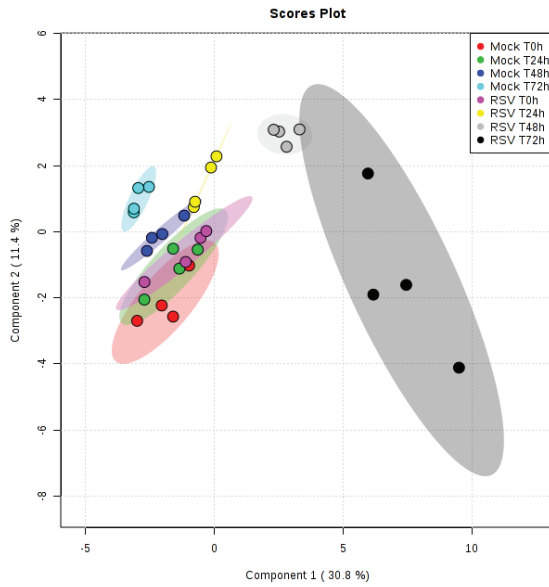


**Figure S5.3:** Supervised partial least squares discriminant analyses of the RSV and Mock infected intracellular amine profile. The PLS-DA shows clustering and initial partial differentiation of the different time points getting more visible 24h post RSV infection.

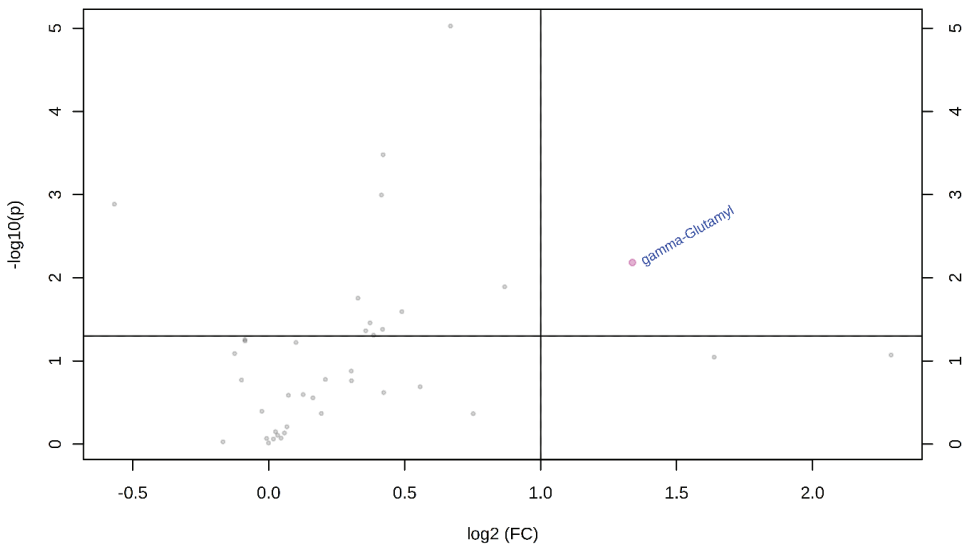


**Figure S5.4:** Volcano plot of  $t = 24h$  RSV vs mock infected A549 cells. The y-axis reflects the metabolite's  $p$  value, plotted to its corresponding FC value on the x-axis.

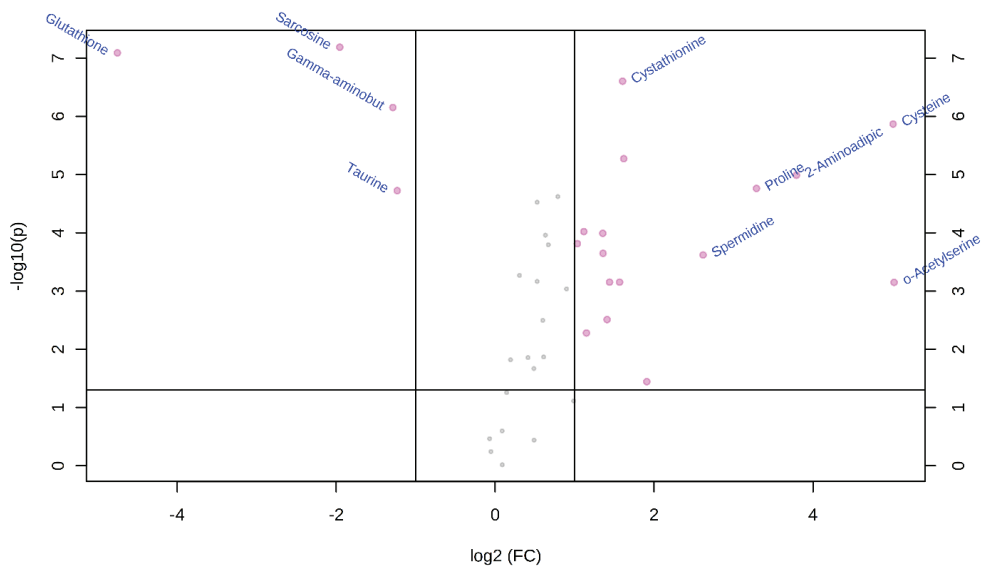


**Figure S5.5:** Volcano plot of  $t = 48\text{h}$  RSV vs mock infected A549 cells. The y-axis reflects the metabolite's  $p$  value, plotted to its corresponding FC value on the x-axis.

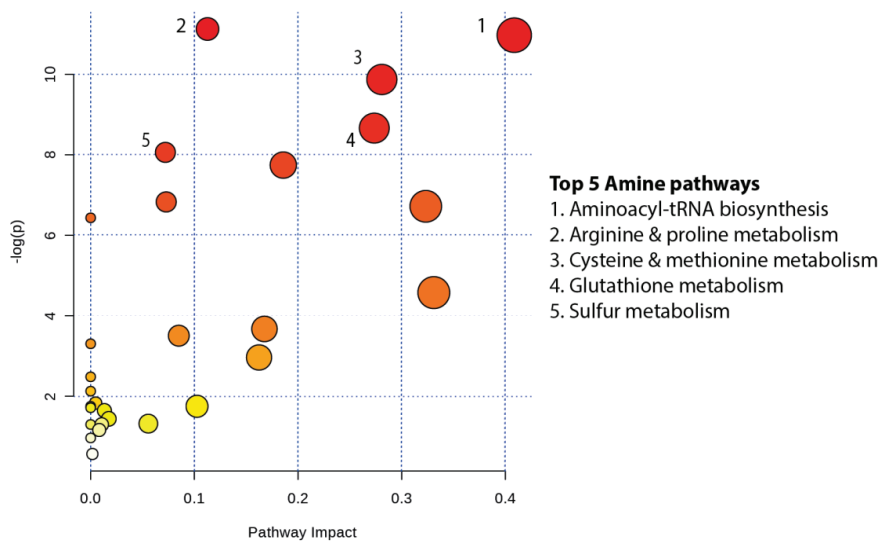


**Figure S5.6:** Pathway analyses of the significant amine metabolites 48h post infection. Metabolites are linked with the Kegg metabolic pathway database (human), with the most affected pathways being identified via the number of hits within each pathway using hypergeometric test & relative-betweenness centrality algorithms.

